Cite this article as:
Suarez, R.G., Miranda, A., Sánchez-Llamazares, J.L. et al. Magnetic Properties of Melt-Spun CoMnSi(B) Alloys. J Supercond Nov Magn 36, 1541–1547 (2023). https://doi.org/10.1007/s10948-023-06597-2

Journal of Superconductivity and Novel Magnetism (2023) 36:1541–1547
https://doi.org/10.1007/s10948-023-06597-2

ORIGINAL PAPER

Magnetic Properties of Melt-Spun CoMnSi(B) Alloys

Rafael G. Suarez[1] · Aida Miranda[1] · J. L. Sánchez-Llamazares[2] · I. Betancourt[1]

Received: 27 March 2023 / Accepted: 3 June 2023 / Published online: 30 June 2023

Abstract
MnCoSi and $MnCoSiB_{0.5}$ alloys were obtained by melt-spinning technique in order to attain polycrystalline microstructures with average grain sizes well below 10 microns. Phase distribution studied by X-ray analysis indicated single-phase materials with orthorhombic structure and TiNiSi-type crystal symmetry. Chemical homogeneity was verified by means of scanning electron microscopy, whereas magnetic behavior corresponded to soft magnetic materials with coercivity values lower than 20 Oe and saturation magnetization of 80 emu/g. Magnetocaloric response of these MnCoSiB alloys was characterized by a maximum magnetic entropy change of 1.0 J/kg K (for a magnetic field variation of 2.0 Tesla) and attractive refrigerant capacity over 100 J/kg, which represents a significant enhancement respect to equivalent MnCoGe alloys.

Keywords Melt-spun alloys · MnCoSi alloys · Magnetic properties · Magnetocaloric response

1 Introduction

Materials with capacity of multi-magnetoresponsive effects are of broad scientific and technological interest due to the associated phenomena related to both, the magnetic order–disorder transition (i.e., Curie transition at a specific temperature T_c), and structural transformations (e.g., martensitic-austenitic transition at a particular temperature T_t), as well as the possibility to couple both phenomena to enhance functional responses such as magnetic field-induced strain, magnetoresistance, shape memory, and magnetocaloric effect [1–6]. In particular, MnCoGe-based alloys have been profusely studied due to the fact that these alloys present a diffusionless martensitic transformation from a low-temperature orthorhombic phase (with TiNiSi-type crystal structure) to a high temperature hexagonal phase (with Ni_2In-type structure) [2, 7]. This transformation occurs at 650 K. On the other hand, both phases present Curie transitions at distinctive temperatures of 345 K and 275 K, respectively. In spite of the good modulability of magnetic and structural properties of MnCoGe alloys [2, 7], a significant disadvantage is their Ge content, because of the high cost and scarcity of germanium metal. Much less attention has been devoted to related MnCoSi alloys, for which T_t transformation goes through above 1100 K, but T_c transition occurs around 350 K, rendering these alloys as an attractive choice for room temperature applications [8–11] In this work, we present and discuss magnetic properties of melt-spun MnCoSiB alloys, as well as their magnetocaloric response.

2 Experimental Methods

Initial ingots of CoMnSi and $MnCoSiB_{0.5}$ alloys were produced by Ar-arc melting in a titanium-gettered atmosphere. Ingots were remelted 4–5 times in order to ensure initial homogeneity. Metallic ribbons were subsequently obtained by chill block melt spinning onto a copper roll by using rotating speeds of 22 m/s (CoMnSi) and 30 m/s ($CoMnSiB_{0.5}$) in a high purity argon atmosphere within a sealed chamber. Phase distribution analysis was performed by X-ray diffraction analysis (XRD) in a Bruker D8 ADVANCE diffraction equipment with Cr radiation ($\lambda = 2.2897$ Å). Further determination of unit cell parameters and crystal structure was carried out by Rietveld fitting. Microstructural features (morphology, grain size, chemical composition) were characterized by scanning electron microscopy (SEM) in a JEOL 7600 F equipment coupled with an energy-dispersive

✉ I. Betancourt
israelb@unam.mx

[1] Departamento de Materiales Metálicos Y Cerámicos, Instituto de Investigaciones en Materiales, Universidad Nacional Autónoma de México., Av. Univ. 3000, Ciudad Universitaria, Ciudad de Mexico C.P. 04510, México

[2] Instituto Potosino de Investigación Científica Y Tecnológica, Camino a La Presa San José 2055, Lomas 4a Sección, San Luis Potosí, S.L.P. C.P. 78216, México

spectroscopy (EDS) unit. Magnetic properties together with magnetocaloric response were studied by means of vibrating sample magnetometry by using a Quantum Design MPMS3 equipment with maximum applied field of 2.0 Tesla. Measurements were made in the plane of the ribbon samples and transverse to the spinning direction so that no correction for self-demagnetization was necessary.

3 Results and Discussion

X-ray diffractograms for MnCoSi and $MnCoSiB_{0.5}$ melt-spun alloys are shown in Fig. 1, including experimental data, Rietveld fitting, and the corresponding difference. All the peaks were identified as reflections of the orthorhombic MnCoSi phase with the following parameters $a = 5.808$ Å, $b = 3.694$ Å, $c = 6.869$ Å, and unit cell volume $V = 147.17$ Å^3 for MnCoSi alloy and $a = 5.791$ Å, $b = 3.697$ Å, $c = 6.873$ Å, and $V = 147.43$ Å^3 for $MnCoSiB_{0.5}$ sample. The slight variation of the unit cell volume of the Boron-containing alloy reflects the incorporation of B atoms into the crystal structure of the MnCoSi phase. Both set of parameters are consistent with those reported in ICDD 00–030-0448 file ($a = 5.819$ Å, $b = 3.691$ Å, $c = 6.853$ Å, and V = 147.1 Å^3). No secondary phases were observed for both alloy compositions.

SEM micrographs for both MnCoSi and $MnCoSiB_{0.5}$ melt-spun alloys are displayed in Fig. 2. A polycrystalline microstructure comprising polyhedral, randomly oriented grains is evident for both samples, with distinctive average grain sizes of 2.13 ± 1.5 microns and of 0.76 ± 1.1 microns for MnCoSi and $MnCoSiB_{0.5}$ alloys, respectively (see distribution histogram for each case). The noticeable grain size refinement for the B-containing alloy can be ascribed to the higher roll speed used for this simple (of 30 m/s compared with 22 m/s of MnCoSi composition), which promotes higher cooling rates and hence, higher number of nucleation sites yielding to reducing mean grain sizes. In addition, due to the very fast extraction of heat, there is no time for crystal growth at any preferred orientation, which in turn leads to random orientation of grains. This fact is supported by XRD measurements, for which no texture was detected for any diffracting plane identified in Fig. 1. The absence of significant microstructural defects (like voids or pores) indicates a well-defined single-phase crystalline structure, consistent with a microstructural homogeneity, which in turn favors a soft magnetic behavior, as discussed in the next section. Chemical homogeneity of alloys was verified by EDS mapping as shown in Fig. 3 for the $MnCoSiB_{0.5}$ alloy, for which no segregation of any atomic species (Mn, Co, Si) is observed, which in turn is consistent with XRD results indicating no secondary phases formation for both alloy samples. The EDS mapping observed for the MnCoSi sample show same features (see Fig. S1 of supplementary material).

Magnetization curves of magnetization M as a function of applied field H are displayed in Fig. 4 for MnCoSi and $MnCoSiB_{0.5}$ melt-spun alloys. A clear soft magnetic behavior is manifested for both samples, with coercivity field H_c values of 4.0 and 12.0 Oe, respectively, as well as saturation magnetization of 80 and 78 emu/g respectively. The

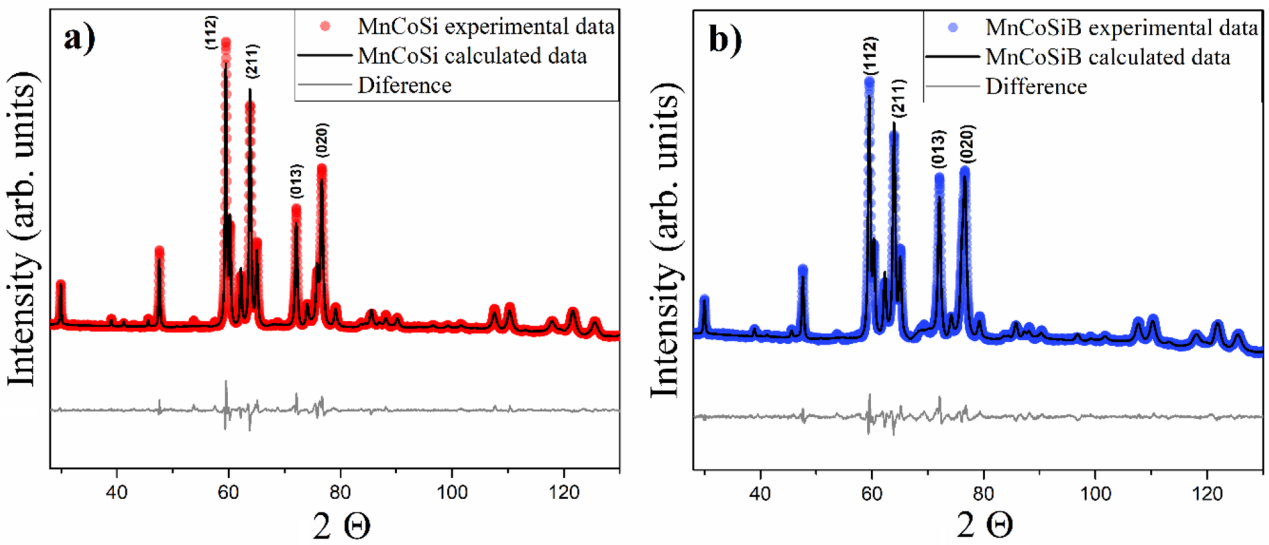

Fig. 1 X-ray diffractograms for **a**) MnCoSi and **b**) $MnCoSiB_{0.5}$ melt-spun alloys. All reflections were associated with orthorhombic MnCoSi phase (only main peaks were labeled with their Miller indices). For both samples, the experimental data is included, together with calculated data and their corresponding difference

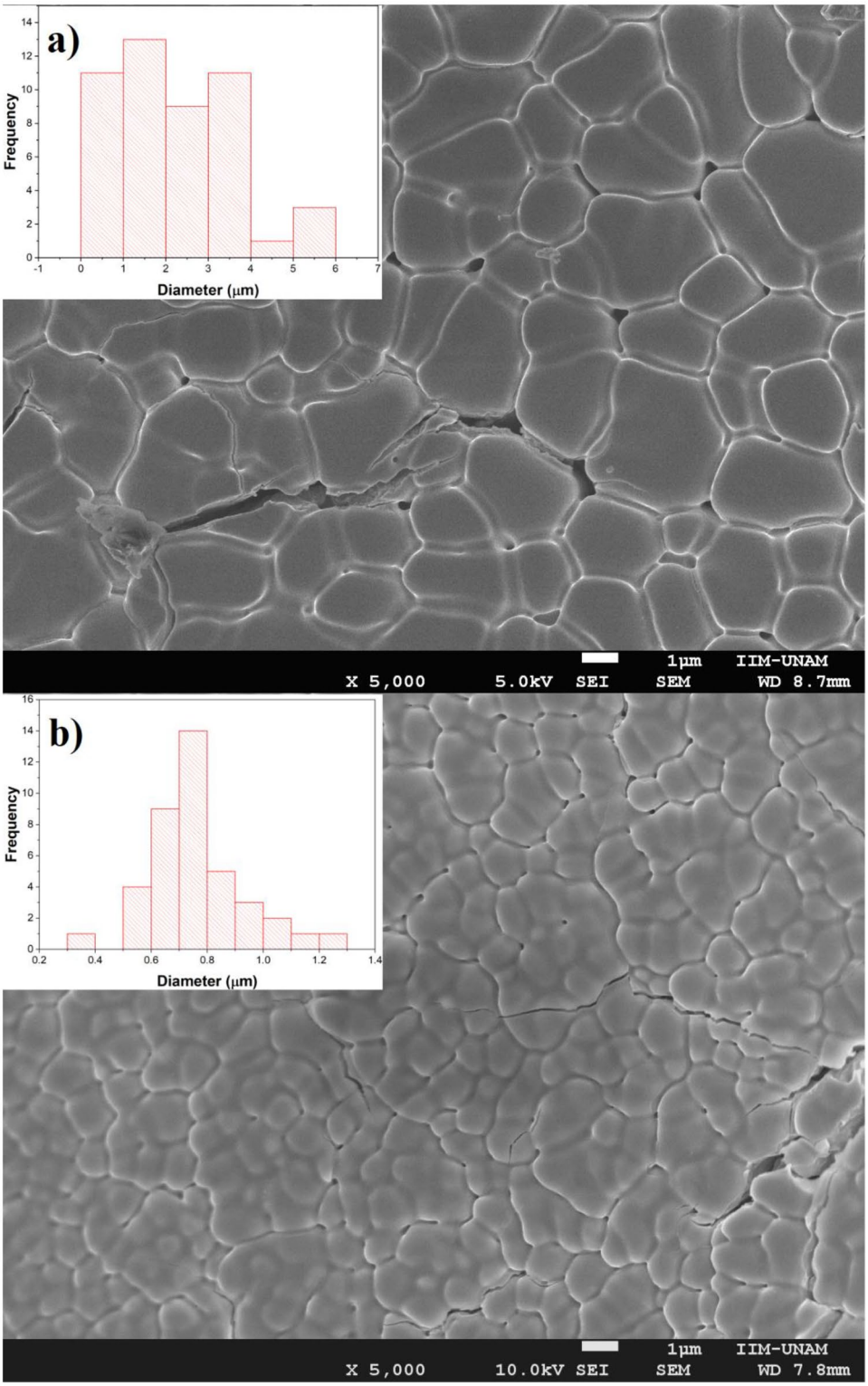

Fig. 2 SEM micrographs for **a**) MnCoSi and **b**) $MnCoSiB_{0.5}$ melt-spun alloys. Main grain sizes are of 2.13 ± 1.5 microns and of 0.76 ± 1.1 microns, respectively

increment of H_c observed for the $CoMnSiB_{0.5}$ alloy can be associated with its grain size refinement since H_c presents a marked dependence with microstructural features and, in particular, with grain size, for which enhanced coercivity values with decreasing grain size in soft magnetic materials has been widely reported [12–14]. In general, low H_c values are consistent with the microstructure homogeneity described in previous section since such structural features facilitate the formation and displacement of domain walls and hence the soft magnetic response characterized for

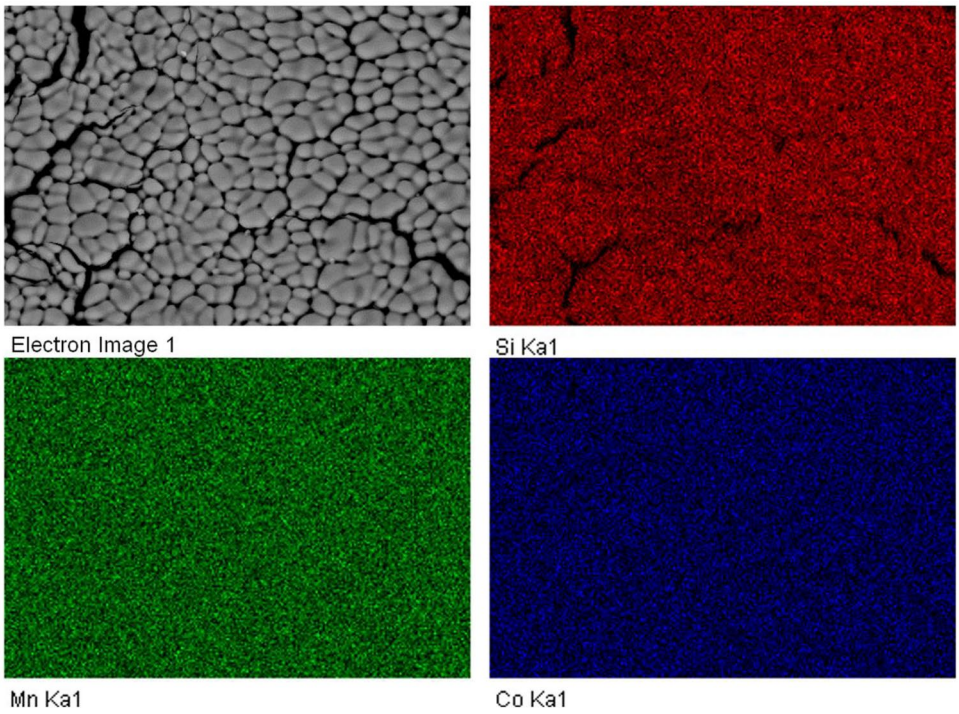

Fig. 3 EDS mapping for the $MnCoSiB_{0.5}$ alloy sample showing chemical homogeneity and single-phase formation

H_c values well below 20 Oe. On the other hand, the slight decrease (2%) observed for the saturation magnetization M_s of the $CoMnSiB_{0.5}$ alloy can be attributed to a dilution effect of the magnetic moment provoked by the inclusion of B atoms into the unit cell structure. This decrement is consistent with the intrinsic nature of M_s, which renders this property as strongly dependent of chemical composition.

Thermomagnetic plots of M as a function of temperature T, for an applied filed $H = 100$ Oe, are displayed in Fig. 5

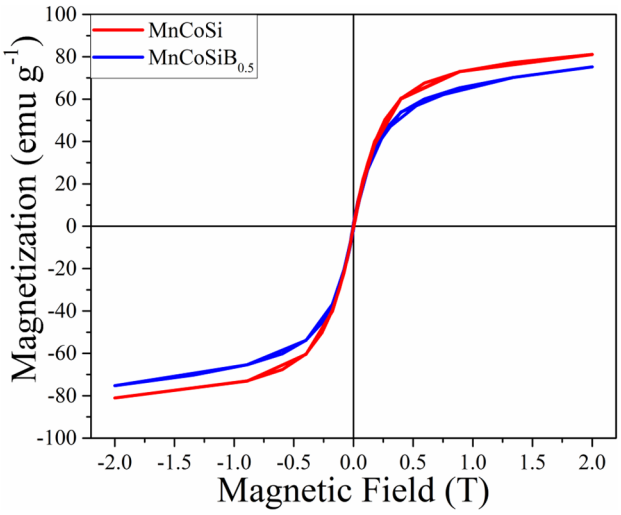

Fig. 4 *M-H* curves for both MnCoSi and $MnCoSiB_{0.5}$ melt-spun alloys showing a characteristic soft magnetic response with very low coercivity fields of 4.0 and 12.0 Oe, respectively and saturation magnetization values of ~ 80 emu/g

for MnCoSi and $MnCoSiB_{0.5}$ melt-spun alloys, showing the Curie transition (T_c) for both samples at 399 and 425 K, respectively (see inset showing a well-defined peak for the derivative dM/dT at both T_c transitions). These T_c values are consistent with those reported for similar alloys, for which an interval of 390–420 K for T_c has been determined [11–16]. The significant difference observed of T_c for the B-containing alloy can be attributed to the incorporation of B atoms into the unit cell structure of the MnCoSi phase, which affects the Co–Co and Mn–Mn interatomic distance, and hence, the exchange interaction determining T_c.

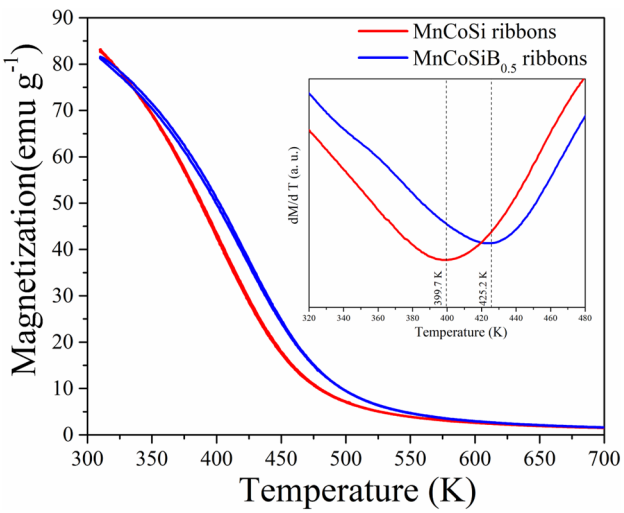

Fig. 5 Thermomagnetic *M-T* (with constant $H = 100$ Oe) plots for MnCoSi and $MnCoSiB_{0.5}$ melt-spun alloys, showing T_c for both samples

On the other hand, isotherms for initial *M-H* curves are illustrated in Fig. 6a, b, for which the ferromagnetic–paramagnetic transition is observed as a progressive linear tendency with increasing temperature. Full linear response indicates the Curie transition. The associated Arrott plots M^2 vs (H/M) (Fig. 7a, b) show a well-defined linear tendency with positive slope at high H values, reflecting the second-order character of the magnetic transition [17].

Within the frame of the modified Arrott plot formalism [18] the equation of state

$$(H/M)^{\frac{1}{\gamma}} = a\frac{T - T_c}{T} + bM^{\frac{1}{\beta}} \quad (1)$$

where a and b are constants and γ and β are the critical exponents, which can be used to identify long-range exchange interactions, in particular, when the fitting exponents γ and β have values of 1.0 and ½, respectively [19]. Such conditions correspond to the Arrott plots of Fig. 7, for which Eq. (1) was fitted with $\gamma = 1.0$ and $\beta = 1/2$. These critical exponents

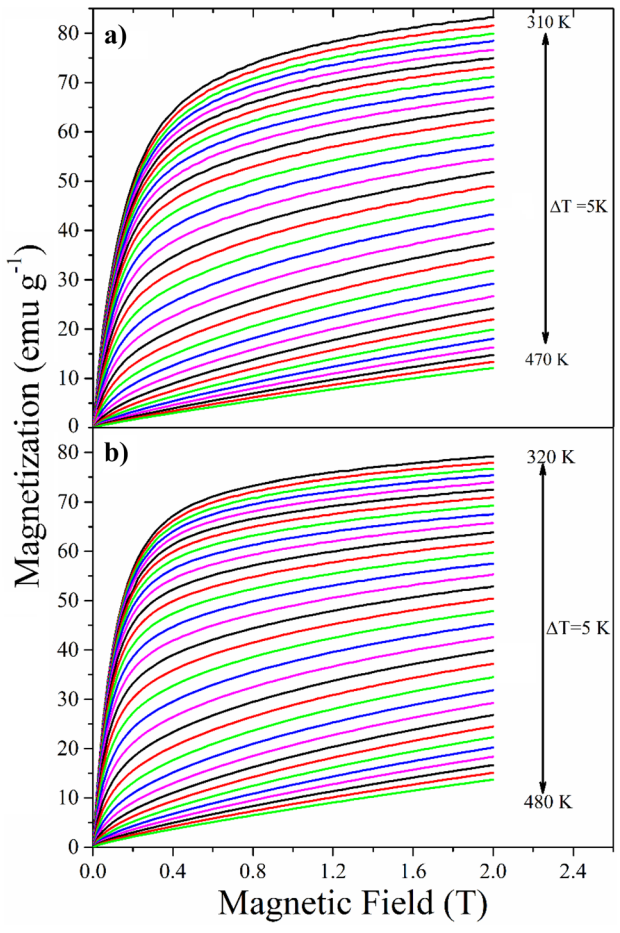

Fig. 6 Initial *M-H* isotherms for **a**) MnCoSi and **b**) $MnCoSiB_{0.5}$ alloy samples

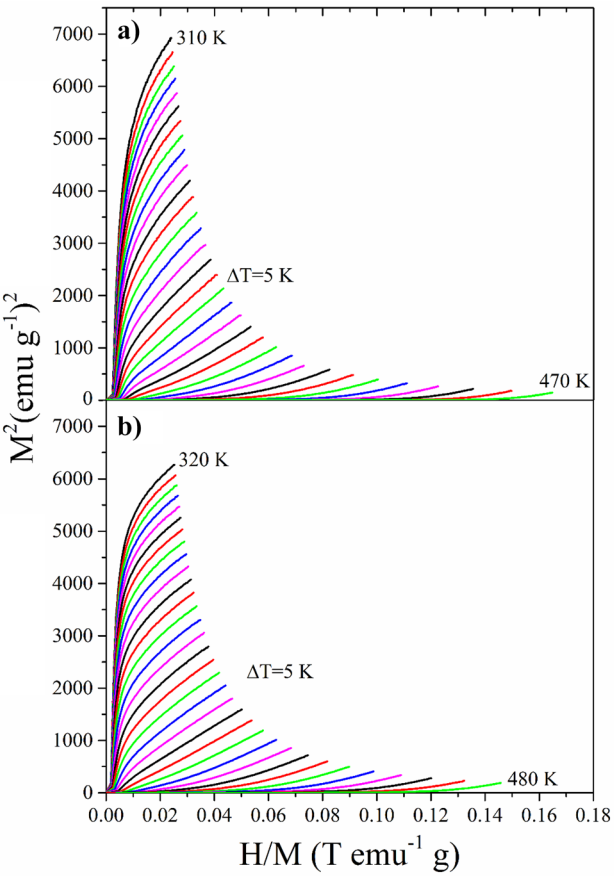

Fig. 7 Associated Arrott plots for **a**) MnCoSi and **b**) $MnCoSiB_{0.5}$ alloys

values indicate consistency with the mean field model, and hence, long-range exchange interactions are expected in our alloys [19], which in turn is congruent with the structural and chemical homogeneity observed by XRD and SEM data.

The magnetocaloric response for MnCoSi and $MnCoSiB_{0.5}$ melt-spun alloys were determined by means of the Maxwell relationships, for which the variation of magnetic entropy ΔS_m as a function of temperature T can be calculated as [20].

$$\Delta S_M = \int_{H_0}^{H_f} \left(\frac{\partial M}{\partial T}\right)_H dH \quad (2)$$

Curves for ΔS_m (T) for both alloy compositions with a variation of applied field $\Delta H = 2.0$ Tesla are displayed at Fig. 8, for which maximum entropy variation ΔS_m^{maxv} for each alloy can be found around 1.0 J/kg K. This moderated response can be ascribed of the pure second-order character of the magnetic transition since such transition occurs at temperatures well below the structural transition reported at 1165 K for this type of alloys [11], and

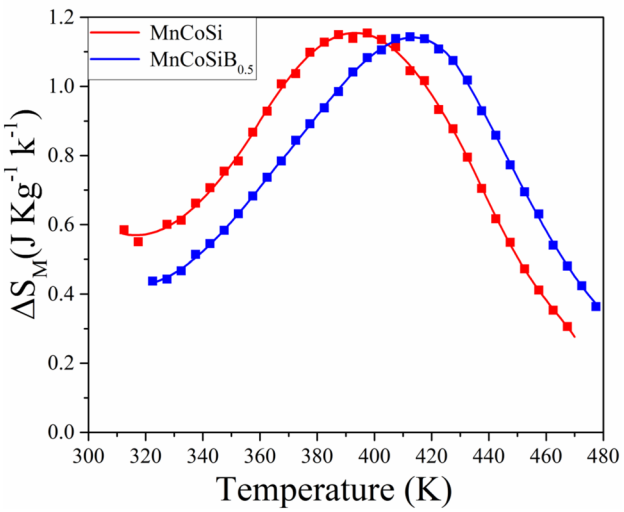

Fig. 8 Magnetic entropy variation ΔS_M as a function of temperature for MnCoSi and $MnCoSiB_{0.5}$ alloys for $\Delta H = 2.0$ T

thus, both transformations events (magnetic and structural) occur uncoupled, yielding to the limited magnetocaloric response observed.

In addition, the refrigerant capacity (*RC*) for both alloys between T_{cold} and T_{hot} sinks (calculated as $RC = (T_{hot} - T_{cold}) \times \Delta S_m^{peak}$), resulted of 108 J/kg and 95 J/kg for MnCoSi and MnCoSiB alloys, respectively. These values compare favorably with those of similar melt-spun MnCoGe alloys (of 90 J/kg)[2]. This property is of particular interest since it represents the capacity of the material to transport thermal energy between T_{cold} and T_{hot} sinks, and hence, *RC* characterizes the alloy ability for technical application as cooling element within a magnetic refrigeration process.

4 Conclusions

The microstructural and magnetic properties of MnCoSi and $MnCoSiB_{0.5}$ melt-spun alloys were characterized by XRD, SEM, and VSM techniques. Single-phase materials were established for both compositions. Magnetic properties were identified as characteristic of soft magnetic materials, with intermediate values of saturation magnetization (of 80 emu/g), low coercivity fields (below 20 Oe), and attractive Curie temperatures between 390 and 430 K. Magnetocaloric evaluation for both melt-spun alloys indicated a maximum magnetic entropy value limited to 1.0 J/kg K, together with a noticeable refrigerant capacity over 100 J/kg. This last property suggests an advantageous ability of our MnCoSiB alloys to transport thermal energy between cold and hot points of a magnetic refrigeration process and thus rendering these alloys as functional materials with potential interest for magnetocaloric applications.

Supplementary Information The online version contains supplementary material available at https://doi.org/10.1007/s10948-023-06597-2.

Acknowledgements I. Betancourt, Rafael. G. Suarez thanks *DGAPA-UNAM* for research support by PAPIIT project IN-104023, whereas Rafael G. Suarez (CVU 557326) and Aida Miranda (CVU 1042641) acknowledge a scholarship support from CONACYT-Mexico. The authors are grateful with Lourdes Bazan for her valuable assistance for SEM observations.

References

1. Hassan, N., et al.: Realisation of magnetostructural coupling and a large magnetocaloric effect in the MnCoGe1+x system. J. Magn. Magn Mater. **439**, 120–125 (2017)
2. Sánchez-Valdéz, C.F., et al.: Magnetocaloric effect in melt-spun MnCoGe ribbons. Scr. Mater. **69**, 211–214 (2013)
3. Franco, V., et al.: The magnetocaloric effect and magnetic refrigeration near room temperature: materials and models. Annu. Rev. Mater. Res. **42**, 305–342 (2012)
4. Franco, V., et al.: Magnetocaloric effect: from materials research to refrigeration devices. Prog. Mater. Sci. **93**, 112–232 (2018)
5. Belo, J.H., et al.: Magnetocaloric materials: from micro-to nanoscale. J. Mater. Res. **34**, 134–157 (2019)
6. Waske, A., et al.: Coupling phenomena in magnetocaloric materials. Energy Technol. **6**, 1429–1447 (2018)
7. Trung, N.T., et al.: Giant magnetocaloric effects by tailoring the phase transitions. Appl. Phys. Lett. **96**, 172504 (2010)
8. Lai, J.W., et al.: Magnetic phase transitions and magnetocaloric effect of MnCoGe1−xSix. J. Magn. Magn. Mater. **372**, 86–90 (2014)
9. Liu, J., et al.: On the magnetic-structure origin of giant magnetostrictive effect in MnCoSi-based metallic helimagnets. Mater. Today Phys. **30**, 100930 (2023)
10. Liu, J., et al.: Enhanced magnetic refrigeration performance in metamagnetic MnCoSi alloy by high-pressure annealing. J. Alloys Compd. **701**, 858–863 (2017)
11. Zhao, J.Q., et al.: Magnetostructural transition and magnetocaloric effect in a MnCoSi-based material system. J. Alloys Compd. **735**, 959–963 (2018)
12. Gong, Y., et al.: Large reversible magnetostriction in B-substituted MnCoSi alloy at room temperature. Scr. Mater. **127**, 165–168 (2017)
13. Chen, J.H., et al.: Structural and magnetic properties of MnCo1−xFexSi alloys. J. Magn. Magn. Mater. **387**, 159–164 (2015)
14. Fang, Y. K. et al.: Structures, magnetic properties, and magnetocaloric effect in MnCo1−xGe (0.02⩽x⩽0.2) compounds. J. Magn. Magn. Mater. **321**, 3053–3056 (2009).

15. Niziol, S. et al.: Magnetic properties of CoMnSi and CoMnSi0.85Ge0.15. Phys. Status Solidi A **51**, K23–K27 (1979).
16. Sandeman, K.G., et al.: Negative magnetocaloric effect from highly sensitive metamagnetism in CoMnSi 1–x Ge x. Phys. Rev. B. **74**, 224436 (2006)
17. Banerjee, B.K.: On a generalised approach to first and second order magnetic transitions. Phys. Lett. **12**, 16–17 (1964)
18. Arrott, A., Noakes, J.E.: Approximate equation of state for nickel near its critical temperature. Phys. Rev. Lett. **19**, 786–789 (1967)
19. Pramanik, A. K., Banerjee, A.: Critical behavior at paramagnetic to ferromagnetic phase transition in Pr0.5 Sr0.5 MnO3: a bulk magnetization study. Phys. Rev. B.- Condens. Matter. Mater. Phys. **79**, 1–7 (2009).
20. Franco, V.: Determination of the Magnetic Entropy Change from Magnetic Measurements: the Importance of the Measurement Protocol. http://www.lakeshore.com/Documents/MagneticEntropyChangefromMagneticMeasurements.pdf. (2014). Accessed 10 Dec 2022